Quantum chemistry and dynamics of the abstraction reaction of H atoms from formaldehyde

A. Siai, I. Oueslati, Boutheina Kerkeni

Quantum chemistry and dynamics of the abstraction reaction of H atoms from formaldehyde

A. Siai[a], I. Oueslati[a,b,c], B. Kerkeni[a,b,d]

[a] *Faculté des Sciences de Tunis, Département de Physique, (LPMC), Université de Tunis El Manar, 2092 Tunis, Tunisia*
[b] *Observatoire de Paris-Meudon, Sorbonne Universités, UPMC Univ Paris 06, UMR8112 du CNRS, LERMA, 5 Place Jules Janssen, 92195 Meudon cedex, France*
[c] *Acadmie Militaire, Fondouk Jedid, 8012, Nabeul, Tunisia*
[d] *Institut Supérieur des Arts Multimédia de la Manouba, Université de la Manouba, 2010 la Manouba, Tunisia*

Abstract

This work reports a reduced dimensionality rate constant calculation of the H-abstraction reaction from formaldehyde. Quantum scattering calculations are performed treating explicitly the bonds being broken and formed. Geometry optimisations and frequency calculations are done at the MP2/cc-pVTZ level while energies are calculated with the CCSD(T) method. An analytical potential energy surface was developed from a relatively small number of grid points. When compared to semi-classical approaches, the quantum scattering calculations show that quantum tunnelling yields large contributions at low temperatures. At 200 K, we note a difference of about 5 orders of magnitude between Transition State Theory (TST) and quantum rate constants. Our predicted results show that the quantum and the CVT/SCT rate constants are in reasonable agreement with the available experiment at high temperatures, but that the last one gives better agreement to experimental results at low temperatures.

Keywords: ab initio, potential energy surfaces, reduced dimensionality, quantum reaction dynamics, kinetics

Email address: Boutheina.kerkeni@obspm.fr (B. Kerkeni)

1. Introduction

Aldehydes are major constituents in the troposphere [1, 2] and especially formaldehyde is among the most reactive organic contaminants. Due to its thermodynamic stability [3], formaldehyde concentration in the polluted areas of the atmosphere can be relatively important [4]. Moreover, these species are among the most abundant interstellar molecules which can be used to trace local physical parameters [5]. It may result from the reaction of atomic hydrogen with carbon monoxide at low temperature on cold grain surfaces, as proposed by previous experimental works [6]. Once H_2CO is formed, it could be the site of many reactions [6, 7, 8], including abstraction reaction by hydrogen atom from formaldehyde:

$$H + H_2CO \rightarrow H_2 + HCO$$

This reaction has been the subject of few experimental studies. The rate constant obtained by Ridley et al. [9] at 297K is expressed as $5.4 \pm 0.5\ 10^{-14}$ cm^3 $molec^{-1}$ sec^{-1}. The measurements of rate constants by Westenberg and deHass [10] and by Oehlers et al. [7] were represented by the following Arrhenius expressions k=2.24 10^{-11} exp[-15.71 (kJ/mol)/RT] for 297<T<652 K and k=1.44 10^{-11} ± 3.16 12^{-12} exp[(-14.5 ± 0.7 (kJ/mol)/RT] for 296<T<780 K (in units of cm^3 $molec^{-1}$ sec^{-1}). Friedrichs et al. [8] have studied the high temperature decomposition of CH_2O. The rate constant for H+CH_2O reaction, determined for temperatures ranging from 1510 to 1960 K is expressed as k=1.1 10^{-9} exp[-40.6 (kJ/mol)/RT] cm^3 $molec^{-1}$ sec^{-1}. On the theoretical side, Goumans et al. [5] used harmonic quantum transition state theory (HQTST) to predict reaction rates for the gas phase reaction of formaldehyde with hydrogen atoms. In their paper, different isotopic combinations were considered and the abstraction reactions were to be preferred over addition reactions in the case of the following isotopic substitutions H/D + H2CO.

Since the reaction involves hydrogen atoms, quantum effects (tunneling and variational effects) are expected to be important at low temperatures. The quantum scattering theory allows for an accurate calculation of rate constants and a thorough understanding of state-to-state dynamics of gas phase reactive collisions. However, going

beyond three atom systems presents a great challenge for exact quantum dynamical approaches. To overcome these difficulties, a reduced dimensionality quantum scattering method [11, 12] has been developed. This approach is based on the idea that only a few degrees of freedom (active modes) contribute significantly to the reaction mechanism while the other degrees of freedom can be treated as spectator modes. The current work makes use of a two dimensional (2D) reduced dimensionality (RD) time independent quantum theory based on the combination of (i) accurate *ab initio* calculations to obtain the required effective potential energy surface (PES) and (ii) the quantum scattering method derived from the bending corrected rotating linear model (BCRLM) of Walker and Hayes [13]. Two active modes are treated explicitly in the scattering calculations while an approximative treatment is made for the remaining internal degrees of freedom (3N-8) via addition of rectilinear-projected zero point energies (ZPE) in the potential surface. This reduced dimensionality approach was successfully employed to study the H-abstraction reaction from small molecules like C1-C3 alkanes and methanol [14, 15, 16, 17] and recently to spin-orbit non adiabatic transitions [18], to n-butane [19], cyclopropane [20] and tetramethylsilane [21].

In order to analyze in details the contribution of quantum effects, we perform also semiclassical tunneling calculations on a ground-state adiabatic minimum energy path (MEP) potential. The rate constants were computed using the conventional transition state theory (TST) [22] with zero curvature tunneling contributions [23] (TST/ZCT) and the canonical variational transition state method (CVT) [24] with small curvature tunneling contributions [25] (CVT/SCT).

This paper is organized as follows. In Section 2, we thoroughly describe the electronic structure calculations and the analytical construction of the PES. In Section 3, some details of the quantum scattering calculations are presented as well as the method used to derive the reaction probabilities and to determine the quantum rate constants. The semi-classical approach based on TST/ZCT and CVT/SCT methods is also given. The results are discussed in Section 4 and compared with the available experimental and theoretical results. Finally, conclusions are given in Section 5.

2. Electronic structure calculations

2.1. Geometry optimization

Equilibrium geometries of the reactants, products and transition state complex are fully optimized at the second order Moller-Plesset perturbation theory level (MP2) [26] with the correlation-consistent polarized valence basis set of Dunning [27], namely cc-pVTZ, using Gaussian 09 [28]. This approach satisfactorily predicts the geometry and the IR spectra [29]. The geometries of reactants, products and transition state for the hydrogen abstraction reaction are listed in Table 1. The interatomic distances and angles are in good agreement with the experimental [31, 32, 33] and past theoretical results [34, 35]. Denoting by H_a the incoming and by H_b the abstracted H-atom (see Fig. 1(a)), we see that during the hydrogen abstraction reaction, the C-H_b bond at transition state (TS) is longer than the equilibrium value by 15%. Similarly, the H_b-H_a bond formed is longer by about 27% in the activated complex compared to the isolated product. The distance of the C- O bond at the transition state is estimated to be 1.179 Å and is shorter than the bond in the isolated formaldehyde molecule (1.210 Å); this phenomenon was also observed by Henon et al. [36] when studying the abstraction reaction of formaldehyde by methoxy radicals. Furthermore, the geometry of TS is almost linear ($\angle$C-H-H=180°) (Fig. 1(a)).

2.2. Vibrational analysis

Harmonic vibrational frequencies of the reactant, products and the transition state species are calculated at the MP2/cc-pVTZ level. All the frequencies are reported in Table 2, as well as the zero point energies (ZPEs). In this work, we didn't use any scaling factor. The comparison of our calculated frequencies to the experimental values shows a good agreement [37, 38, 39]. From this table, we note the presence of a single imaginary frequency for the transition state which confirms the presence of a first order saddle point for the studied reaction. Moreover, we obtain positive frequencies for both reactant and products indicating that these are local minima.

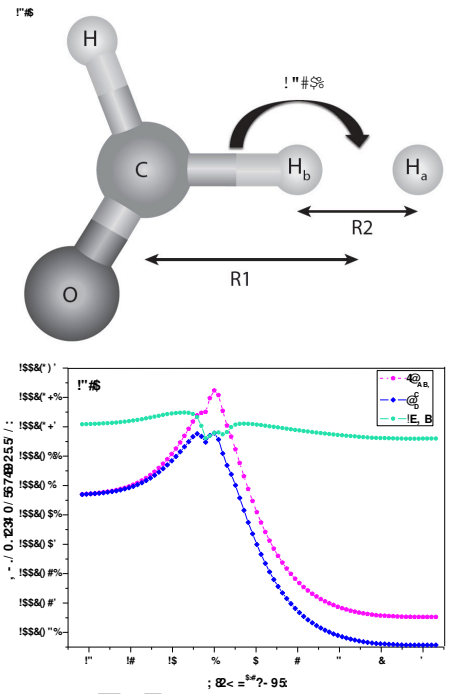

Figure 1: **(a)** : Optimized geometry of the transition state at the MP2/cc-pVTZ level.The value of the angle involved in the reaction is shown. **(b)** Minimum energy path (V_{MEP}), vibrational adiabatic potential energy (V_a^G), and ZPE of 3N-6 vibrational mode

as functions of (s) (amu$^{1/2}$ a_0) at the CCSD(T)/cc-pVTZ//MP2/cc-pVTZ level.

Table 1: Molecular geometry parameters of the fragments (bond lengths (Å) and angles (°)) at the MP2/cc-pVTZ level. H_b is the abstracted atom, while H_a is the incoming atom.

Species	Methods/Basis	CO	CH	CH_b	$\angle H_bCO$	H_aH_b	$\angle HCH_b$	$\angle H_aCH_b$
H_2CO	MP2/cc-pVTZ	1.210	1.100	1.100	121.9	-	116.1	-
	HF/6-31G**[34]	1.189	1.094	-	-	-	116.2	
	MP2/6-31G**[34]	1.219	1.099	-	-	-	115.52	
	Exp. [31]	1.203	1.099	-	-	-	116.5	
TS	MP2/cc-pVTZ	1.179	1.110	1.293	125.3	1.008	112.3	179.7
HCO	MP2/cc-pVTZ	1.182	1.117	-	124.0	-	-	-
	CCSD/acvqz [35]	1.176	1.118	-	124.61	-	-	-
	CCSD/CBS [35]	1.174	1.117	-	124.6	-	-	-
	Exp. [32]	1.198	1.080	-	119.5	-	-	-
H_2	MP2/cc-pVTZ	-	-	-	-	0.737	-	-
	Exp. [33]	-	-	-	-	0.741	-	-
R-vdW	MP2/cc-pVTZ	1.210	1.100	1.100	121.9	3.351	116.18	-

Table 2: Calculated vibrational frequencies (in cm^{-1}) and zero-point energies (in hartree) for the stationary points. Transition state frequencies are given prior to (pre) and after (post) rectilinear projection of explicitly treated vibrational modes.

	Methods/Basis	Frequency (cm^{-1})	ZPE
H_2CO	MP2/cc-pVTZ	1210 1281 1554 1773 2967 3040	0.026936
	HF/6-31G** [34]	1335 1368 1656 2008 3227 3149	
	MP2/6-31G** [34]	1219 1298 1589 1796 3108 3030	
	Expt. [37]	1167 1249 1500 1746 2843 2783	
HCO	MP2/cc-pVTZ	1122 1930 2752	0.013223
	CCSD(T)/acvqz [35]	1117 1899 2714	
	CCSD(T)/CBS-1b [35]	1120 1905 2717	
	Expt. [38]	1126 1920 2790	
H_2	MP2/cc-pVTZ	4525	0.010308
	Expt. [39]	4403	
TS: pre-projected	2149*i* 347 388 1176 1269 1377 1428 2382 2923		0.025717
TS: post-projected	0 347 388 1176 1269 1377 2381 2922		0.022520

2.3. Energetics

The computed energetics are the vibrational adiabatic barrier (ΔV_a) and the enthalpy of reaction (ΔH) including the difference of zero-point vibrational energy (ΔZPE) between the transition state and the reactants and between the products and the reactants, respectively. The calculations lead to ΔV_a = 6.69 kcal/mol and to a reaction exothermicity of -16.41 kcal/mol at the CCSD(T,full)/cc-pVTZ level [40]. To validate the current methodology, energy calculations for stationary points were also performed at the CCSD(T)-F12a/VTZ-F12 level [41] for which the F12 correction strongly improves the basis set convergence of correlation and reaction energies [41]. The computations led to a barrier height of 6.68 kcal /mol and exothermicity of -16.38 kcal/mol, respectively. The calculated enthalpies of reaction are in good agreement with Ruscic result [42] (-16.55 0.002 kcal/mol at 0 K).

The calculated adiabatic vibrational barrier height is found to be in agreement with theoretical values [5] which are estimated to 7.18 kcal/mol at the CCSD(T)/CBS level and to 6.08 kcal/mol at the BB1K/6-311+G** level, respectively. Furthermore, ΔV_a lays above and below the values obtained in experiments (3.46 [7], 3.75 [10] and 9.70 [8] kcal/mol). This difference (even between experimental values) could be explained by the fact that in the experiment, the activation barrier is obtained from a fit of the temperature-dependent kinetic data to an Arrhenius functional form that also depends on many factors such as the data quality and the temperature range considered in experiment.

Two van der Waals complexes in the reactant and product sides were identified (R-vdW and P-vdW). The well depths of R-vdW relative to reactants and of P-vdW relative to products are 0.341 and 0.376 kcal/mol at MP2 level, respectively. When taking the BSSE correction into account, the energies of the weakly bonded complexes become 0.337 and 0.078 kcal/mol, respectively. Consequently, P-vdW is not electronically stable, hence the MP2 binding energy is due to BSSE. Table 1 reports the geometry of the R-vdW complex. However, this complex is described by a very small depth (0.229 kcal/mol at the CCSD(T) level), therefore, we expect that it would not play an important role on the dynamics of the studied abstraction reaction.

2.4. Minimum energy path

The MEP was obtained from IRC calculations [43] as implemented in Gaussian 09 [28]. For each point along the MEP, the frequency was computed at the MP2/cc-pVTZ level and the energy was further refined at the CCSD(T)/cc-pVTZ level. An improvement of this energy has been proposed by adding the ZPE correction of 3N-6 vibrational modes. Figure 1(b) displays the variation of the classical potential energy (V_{MEP}) as a function of the reaction coordinate (s) is plotted. From this figure, we note that the shape of the ZPE curve has a notable effect on the vibrational adiabatic potential energy (V_a^G) curve shape. Indeed, it presents two humps (a hump at s= -0.8 Bohr, a hollow at s=-0.5 Bohr and a hump at s = 0 Bohr) as previously found for the CH_3F + HCl reaction [44]. The maximum is still located at s=0 Bohr as in the case of V_{MEP}. There is no shift with respect to the saddle point on V_{MEP}.

Since the shapes of the V_a^G and V_{MEP} curves are different, the variational effect is expected to be important in evaluating the rate constants for the H+H_2CO reaction. Despite this finding, the classical potential energy and the vibrational adiabatic potential energy (V_{MEP} and V_a^G) have the same maximum located at s=0 Bohr.

In order to calculate the semi-classical rate constants, a curvilinear projection operator [45] is applied, as implemented in POLYRATE2010 program [46], to project the reaction coordinate out of the Hessian matrix of the system.

2.5. Effective Potential energy surface

The studied reaction is of the form: H_a + H_bCZ → H_aH_b + CZ, where C is the species from which the H_b atom is abstracted. As shown in paragraph (2.1), the three atoms H_aH_b-C involved in the reaction have a quasi-collinear geometry so that the 2D model is well suited. In Figure 1(a), the distances connecting atoms involved in the reaction, describing the formation and breaking chemical bonds. The latter are defined by the Jacobi coordinates R1 and R2, where R1 is the distance between the centre of mass of H_a + H_b and the centre of mass (COM) of CZ and R2 is the distance between H_a and H_b. In order to reduce the complexity in calculating the centre of mass of the reactants, we assumed that the COM of the H_2CO is situated on the carbon atom from which the H atom is abstracted.

The reduced dimensionality 2D potential energy surface for $H+H_2CO$ reaction is given using hyperspherical coordinates (ρ, δ) defined from the Jacobi coordinates (R1, R2): [14]

$$\frac{M_1}{\mu}(R1)^2 = [\rho\ cos(\delta)]^2 \qquad \frac{M_2}{\mu}(R2)^2 = [\rho\ sin(\delta)]^2 \tag{1}$$

$$M_1 = \frac{(m_{H_a} + m_{H_b})(m_C + m_H + m_O)}{3m_H + m_O + m_C}$$

$$M_2 = \frac{m_{H_a} \times m_{H_b}}{m_{H_a} + m_{H_b}}$$

$$\mu = (M_1 M_2 M_3)^{1/3} \tag{2}$$

M_3 is the reduced mass of the product :

$$M_3 = \frac{(m_H + m_C)(m_O)}{m_H + m_O + m_C}$$

The (ρ, δ) coordinates present the advantage to describe more easily particle arrangements.

In order to map the reactive domain, an adequate number of grid points (R1, R2) was chosen. Fifty (50) *ab initio* points were required for the PES. At every grid point, we used the following procedure :

-Geometry optimisations and frequency calculations at the MP2/cc-pVTZ level.

-Spectator ZPE calculation: the rectilinear projection method [47, 48] was used to remove out the contributions of the two active vibrational modes from the hessian. Transition state frequencies prior to and post projection are given in Table 2. One of the frequencies projected out is the imaginary normal mode. For the remainder vibrational modes, the pre-projected frequencies are almost unchanged.

-Single Point Energy Correction: addition of ZPEs of 3N-8 spectator vibrational modes to CCSD(T) energies to provide the effective potential energy for further dynamics calculations.

-Surface fitting: the *ab initio* data is fitted to an analytical expression, developed in a

previous work [14]. This functional depends on 31 parameters and is defined as the sum of two Morse functions which are oriented in opposite directions and separated by an energy barrier. Nonlinear least squares techniques were used based on the Gauss-Newton method [49] in order to find the suitable parameters. An adequate potential fit was obtained with a the sum of square residuals of 2.5×10^{-4}.

The functional is given in atomic units by:

$$
\begin{aligned}
V(\rho,\delta) \;=\; & [0.150043 + (-2.416258(E-8) - 0.028146 \times \rho^{(-4.338097)})(\exp(0.280155 \times \rho))] \\
& \times [[1. - \exp(((6.298016 + 0.173671 \times \rho + 0.042166 \times \rho^2) \times \delta \\
& + (1.116035 - 0.067888 \times \rho - 0.033270 \times \rho^2) \\
& - ln(-35.827604 + 19.681085 \times \rho - 0.029212 \times \rho^2)))]^2 + 367.949226] \\
& + [4.334289 + (8.123435(E-4) - 4.264437 \times \rho^{(-0.017359)}) \exp(0.001261 \times \rho)] \\
& \times [[1. - \exp(-((2.282739 + 1.833952 \times \rho + 0.006280 \times \rho^2) \times \delta \\
& + (-11.214785 - 0.150228 \times \rho + 0.006246 \times \rho^2) \\
& + ln(7158.571 + 4896.161325 \times \rho - 187.325218 \times \rho^2)))]^2 \\
& - 0.394825] + 55.089878 \qquad (3)
\end{aligned}
$$

This functional is valid for $2.5 \leq \rho \leq 24$ a.u. and for $0 \leq \delta \leq \delta_{max} = 0.80$ rad. Fig. 2(a) shows a contour plot of the fitted potential energy surface. The hyperspherical coordinates at the saddle point are ρ= 3.358 a.u. and δ=0.28 rad. The plot indicates a local minimum at ρ= 6.185 a.u. and δ=0.56 rad, which corresponds to the R-vdW complex. Figure 2(b) illustrates the good agreement between the calculated *ab initio* energies and the fit given by Eq. (3) for two values of the hyperspherical coordinate ρ=3.538 a.u. corresponding to the transition state and ρ=24 a.u. in the asymptotic region. For the latter, the PES is defined by two potential wells : the first one around δ = 0.73 rad describing the area of the broken C-H_b bond and the second around δ = 3 10^{-2} rad describing the formed H_b-H_a bond.

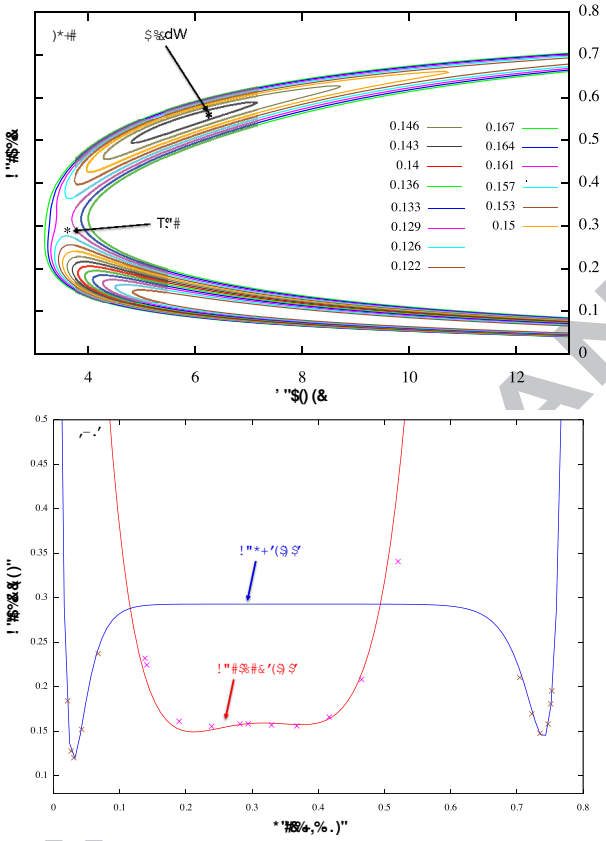

Figure 2: **(a)** Contour plot (line) of the fitted potential V (ρ, δ) as function of ρ et δ. The positions of the TS and the R -vdW complex are marked on the plot with arrows. **(b)** Fitted V(ρ,δ) (full line) and *ab initio* grid data (cross) for ρ=3.538 a.u. and ρ=24.00 a.u., respectively. Energies are in Hartree.

3. Dynamics

The Hamiltonian for a reduced dimensionality (2D) system is written in terms of the hyperspherical coordinates (ρ, δ) based on the BCRLM method : [13]

$$\hat{H} = -\frac{\hbar^2}{2\mu}\frac{\partial^2}{\partial\rho^2} - \frac{\hbar^2}{2\mu\rho^2}\frac{\partial^2}{\partial\delta^2} + \frac{3\hbar^2}{8\mu\rho^2} + \frac{\hat{J}^2}{2\mu\rho^2} + V(\rho,\delta) \tag{4}$$

where $\hat{J}$ is the total angular momentum and V (ρ, δ) is the effective potential energy surface that includes zero point energies relative to the contribution of the 3N-8 spectator vibrational modes. The R-matrix propagation algorithm developed by Walker and coworkers [50, 51] to solve close coupled equations was used. The hyper-radius ρ is first divided into N_ρ sectors in the range $[\rho_{min}, \rho_{max}]$. At fixed $\rho = \rho_k$, the wave function is expanded as:

$$\Psi_\nu(\rho,\delta;\rho_k) = \sum_{\nu}^{N} f_{\nu\nu'}(\rho;\rho_k) \sum_{n_\delta}^{N_\delta} c_{n_\delta}^{\nu} \psi_{n_\delta}(\delta;\rho_k) \tag{5}$$

ν and ν' refer to the quantum vibrational states relative respectively to the initial (C-H_b) and final (H_b-H_a) bonds, N_δ is the number of sectors obtained by dividing the range of values of δ defined in the range of [0, δ_{max}=0.80 rad], $f_{\nu\nu'}$ is the radial function that depends on ρ. ψ_{n_δ} is the eigenvector of the Hamiltonian $\hat{H}_\delta$ written as:

$$\hat{H}_\delta = -\frac{\hbar^2}{2\mu\rho_k^2}\frac{\partial^2}{\partial\delta^2} + V_\delta(\delta;\rho_k) \tag{6}$$

where $V_\delta(\delta;\rho_k)$ is the potential energy obtained for a given ρ_k. Using a discrete variable representation with a particle-in-a-box basis set, the diagonalization of this Hamiltonian gives eigenenergies called hyperspherical adiabats $\epsilon(\rho_k)$. They correspond to the energies of the vibrational states for a given value of ρ_k and $\psi_{n_\delta}(\delta;\rho_k)$ eigenvectors.

In the asymptotic region, for ρ_k ranging from ρ_a=20 a_0 to ρ_b=24 a_0, approximate boundary conditions are applied to obtain sector scattering matrix elements $S_{\nu\nu',k}(E)$ between all energetically allowed states. The average of $|\, S_{\nu\nu',k}(E)\,|^2$ over sectors gives the state to state probabilities $P^{J=0}_{\nu\nu'}(E)$ from an initial ν to a final ν' vibrational state. The cumulative probability is obtained as:

$$P^{J=0}_{cum}(E) = \sum_{\nu}\sum_{\nu'} P^{J=0}_{\nu\nu'}(E) \tag{7}$$

The calculations are checked carefully to ensure converged reaction probabilities with respect to the scattering parameters given in Eq. (3). The R-matrix is propagated over N_ρ = 135 sectors from ρ_{min} = 2.5 a_0 to ρ_{max} = 24.0 a_0. For each sector, $\hat{H}_\delta$ is diagonalized employing a primitive basis of N_δ = 130 particle-in-a-box wave functions. A contracted basis set of N = 10 channels is used.

The reaction rate constant, $k_{RD}(T)$, is then calculated using the cumulative reaction probability with the energy and J-shifting approximations [12, 52] :

$$k_{RD}(T) = \frac{Q^{\#}(T)}{hQ^{H_2CO}(T)Q^{H}(T)} \int_0^\infty dE P_{cum}^{J=0} e^{-E/k_BT} \tag{8}$$

$Q^{\#}$, Q^{H_2CO} and Q^{H} are respectively the transition state (TS) and the reactants partition functions. Only the frequencies of vibrational spectator modes (3N-8) are included in the vibrational partition function of the TS.

For comparison purposes, we computed also the rate constants, k_{TST} from transition state theory and k_{CVT} from variational transition state theory: [24]

$$k_{TST}(T) = \frac{Q^{\#}(T)}{hQ^{H_2CO}(T)Q^{H}(T)} \times k_BT \times e^{-\Delta V_a/k_BT} \tag{9}$$

$$k_{CVT}(T) = \sigma \frac{k_BT}{h} K^0 exp[-\Delta G(T, s^{*,CVT})/k_BT] \tag{10}$$

where $s^{*,CVT}$ is the location of the canonical transition state on the reaction path, $\Delta G(T, s^{*,CVT})$ is the free energy of activation and K^0 is the reciprocal of the standard-state concentration, taken as 1 molecule cm^{-3}.

Two H abstraction sites are accounted for via the symmetry number (σ) in equation (10). The rotational partition function used in the calculation of the total partition functions in equations (8) and (9) are written according to σ. The expression of the rotational partition functions can be found in ref. [53]. The imaginary reaction coordinate frequency is removed, so that the total number of vibrations in the partition function reduces to 3N-7.

Since the system involves a transfer of light atoms like the H atom, we expect important tunneling and variational effects at low temperatures. In the ZCT and SCT approaches, tunneling is calculated from the semi-classical (i.e. WKB) ground state transmission

coefficient $\kappa(T)$ [25]:

$$k_{ZCT}(T) = \kappa_{ZCT}(T) \times k_{TST}(T) \tag{11}$$

$$k_{SCT}(T) = \kappa_{SCT}(T) \times k_{CVT}(T) \tag{12}$$

The detailed description of the $\kappa(T)$ calculations can be found in ref. [24, 25, 53]. These semi-classical rate constants were computed using the POLYRATE program, version 2010-A [46].

4. Results and discussion

4.1. Reaction probabilities

Figure 3(a) presents the variation as function of the translational energy of the ground state of H_2CO of the cumulative quantum reaction probability, calculated for a total angular momentum $J = 0$, for two initial vibrational states ($\nu = 0$ and 1) of H_2CO, summed over all H_2 ν'-vibrational states. The energy variation of the total cumulative reaction probability (CRP) summed over all reactants and products is displayed in Fig. 3(b). The position of the barrier also shown in Fig. 3(b) highlights the importance of quantum tunneling to the reaction process. The reaction probability grows rapidly for translational energy around 0.23 eV until it exceeds 1 at 0.56 eV. Fig. 3(b) presents broad oscillations for increasing energies as found in previous works [14, 15, 18, 17, 21]. The largest contribution to the cumulative reaction probability is mainly from the ($\nu = 0$) vibrational mode at energies of interest (see Figure 3(a)). This mode has a smaller threshold energy than the ($\nu = 1$) one.

In Figure 4, we display the state-to-state reaction probabilities noted $P_{\nu\nu'}$. We notice that the contribution of the transition from the initial reactant state ($\nu = 0$) to the final product state ($\nu' = 0$) to the cumulative reaction probability is the major one at the energy of 0.23 eV. Then, it decreases with increasing translational energy. The magnitude of the ($0 \rightarrow 1$) transition which appears at 0.3 eV becomes more significant after 0.9 eV. For the first vibrationally excited reactant state ($\nu = 1$), the reaction probabilities to the product states ($\nu' = 0$) and ($\nu' = 1$) have comparable thresholds but the magnitude of the second one is higher than the first one. A translational energy of 0.53 eV

is required to obtain H_2 in its the excited ($v' = 2$) state. The ($1 \rightarrow 2$) transition has the largest contribution compared to the reaction probabilities from the ground state ($v = 0$) and the second excited ($v = 2$) reactant state. Tunneling effects are important for H+H_2CO reaction, since there is a non-zero contribution to the CRP which starts at 0.23 eV, while the vibrational adiabatic barrier on the PES of the 2D model is 0.29 eV.

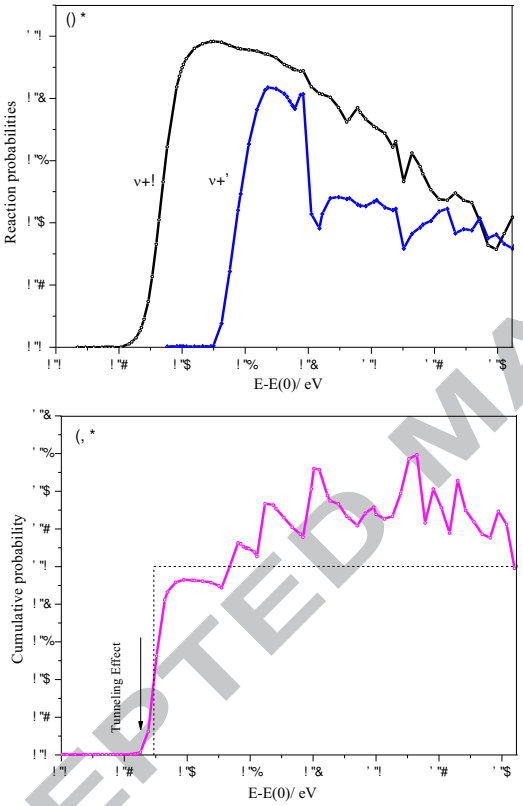

Figure 3: (a) Initial state-selected and (b) cumulative reaction probabilities for total angular momentum $J = 0$, as a function of translational energy of the (H_2CO $v = 0$) initial ground state. The black dashed line is the classical reaction probability obtained from the adiabatic 2D energy barrier (0.29 eV).

4.2. Rate constants

Thermal rate constants were computed over the temperature range [200-2000 K] using the formalism of reduced dimensionality quantum dynamics to obtain $k_{Quantum}$

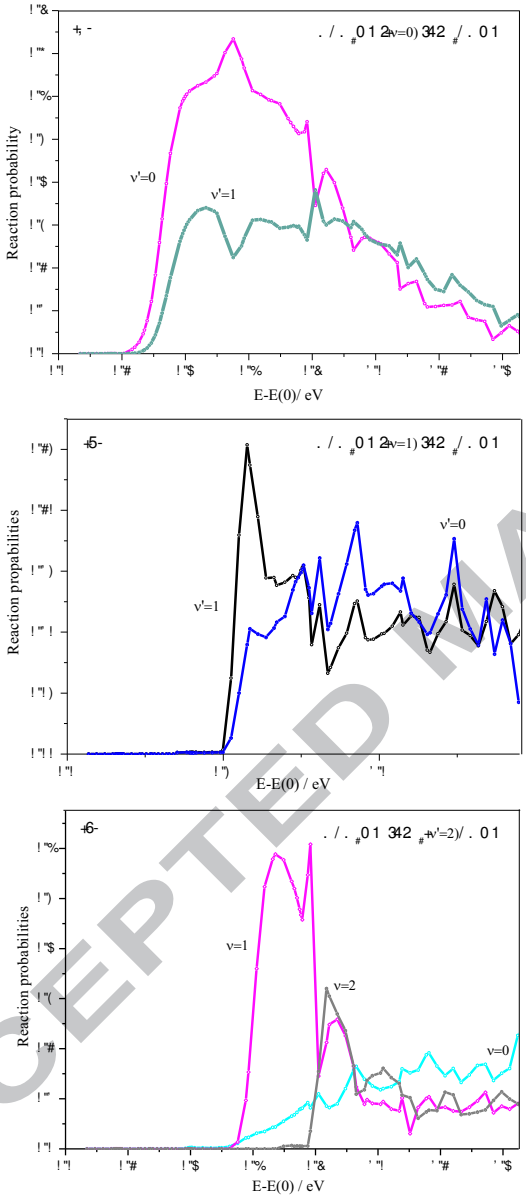

Figure 4: State-to-state reaction probabilities of the H+H_2CO (v) → H_2 (v') +HCO reaction for various values of v and v' as a function of translational energy of the (v = 0) initial ground state for a total angular momentum quantum number J = 0: (a):v = 0; (b):v = 1; (c):v' = 2.

(T). In addition to experimental data, we compare our quantum scattering results with TST/ZCT and CVT/SCT results. The logarithm of the calculated k_{TST}, k_{CVT}, $k_{TST/ZCT}$, $k_{CVT/SCT}$ and $k_{Quantum}$ rate constants and the available experimental and theoretical data are plotted against 1000/T in Figure 5.

Over the whole temperature range, similar results are obtained from the CVT and TST methods. The ratio k_{CVT}/k_{TST} takes the values 0.92 and 0.94 at 1000 and 2000 K, respectively. According to these calculations, the variational effects seem to be small at large temperatures. Furthermore, the quantum and TST curves cross each other at 800K : the ratio k_{RD}/k_{TST} is equal to 0.78 and 0.6 at 1000 and 2000 K, respectively. These results suggest that quantum dynamics methods highlight at high temperatures a recrossing effect (recrossing of trajectories in the transition state region) which k_{CVT} may underestimates [54] and k_{TST} neglects. In fact, the effect of barrier recrossing is reduced in variational transition state theory by letting the TS deviate from the saddle point in the dividing surface, and optimizing its position by searching for the free energy maximum along (s) in the canonical ensemble (CVT) [25] .

At low temperatures, the classical TST method underestimates the rate constant compared to experimental values. The quantum scattering and the (CVT/SCT) results exhibit a curvature with respect to the TST rate constants. This effect increases as the temperature decreases. This behavior indicates that there are large quantum effects at low T. In fact, tunneling plays an important role as noted by the transmission coefficients : 37017, 2213 and 133 for k_{RD} and 10240, 710 and 62 for k_{SCT} at 200, 240, 300 K, respectively. This is expected since tunneling effect was found in the reaction probability calculations (Fig. 3(b)).

Our results were compared to the theoretical one computed by Goumans et al. [5]. In this previous work, the rate constants were calculated for the temperature range [500-20 K] using the harmonic quantum transition state theory (HQTST). This rate is clearly lower than k_{RD} and $k_{CVT/SCT}$ and it slightly exceeds $k_{TST/ZCT}$ which seriously underestimates rate constants at lower temperatures.

We also show in Fig. 5 experimental results reported at 297 K by Ridley et al. [9], at 297-652 K by Westenberg and deHass [10], at 296-780 K by Oehlers et al. [7] and at 1510-1960 K by Friedrichs et al. [8]. As we can see in the inset of Figure 5, the

quantum and the CVT/SCT results are in relatively good agreement with the experimental results, at high temperatures. However, at low temperature the rate constant is better represented by the CVT/SCT model than the quantum one. In fact, the temperature variation of $k_{Quantum}$ exhibits a more pronounced curvature and deviate from experimental results.

Such behavior, also found for other systems [19, 21], could be due to the application of the rectilinear coordinate projection method used for removing the contribution of the two active modes from the Hessian [16, 17, 55]. An improvement of the results can be made with the use of curvilinear coordinates [16] to remove the contribution of nonzero gradients from the Hessian matrix and leads to better thermal rate constants. In the future, we may consider studying this reaction with higher dimen- sionality and the possible occurence of CH3O and CH2OH complexes and their influence on the proceeding of this reactive mechanism.

5. Conclusion

The aim of this study was to provide a detailed understanding of the gas phase H+H_2CO abstraction reaction. This is the first quantum study for this system for which no analytical potential energy surface was available and for which tunneling is important since the transfer of a hydrogen atom is involved. We have used a reduced quantum dynamics (2D) model to compute the reaction probabilities and the thermal rate constants. Selected state-to-state rate constants were also computed. An *ab initio* effective potential energy surface was developed from a minimal number of grid points, it takes into account the harmonic zero point energies of the spectator modes. The 2D model showed that H_2 is mainly formed in its ground vibrational state (v'=0). However, reaction from the vibrationally excited states of H_2CO (v=1) is not negligible. Comparison of thermal rate constants with experiments shows a reasonable agreement. The CVT/SCT rate constant model seems to give the better agreement to experimental results at low temperatures compared to quantum rate constants. Improvement of the quantum results may be obtained through the use of curvilinear internal coordinates to

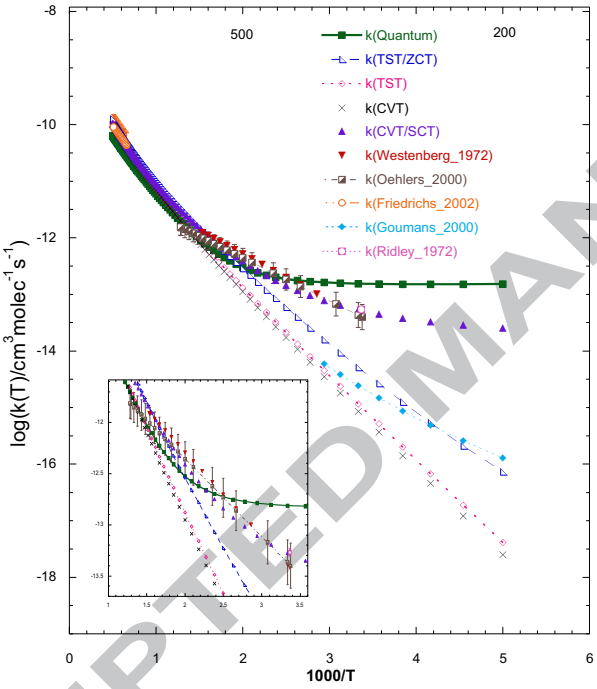

Figure 5: Comparison of the quantum thermal rate constants with the semiclassical TST and CVT/SCT (this work), HQTST [5] and experimental [7, 8, 9, 10] results. The inset is a portion of the main plot showing the variation of rate constants for temperature range [278-1000 K].

determine the frequencies of the spectator modes from the Hessian. However, it could be useful for new experimental work to be performed on the H_2CO + H-abstraction reaction especially at low temperatures. Improving the treatment of the electronic structure computations and the dynamics studies are in progress.

6. Acknowledgements

We wish to thank Prof. N. Feautrier for fruitful discussions and for critical reading of the manuscript. The calculations were performed at the IDRIS and CINES French National Computer centres under projects 2012046838 and 2013046838. The authors would like to thank Professor Donald G. Truhlar for providing the POLYRATE program, version 2010-A.

References

References

[1] J. H. Seinfeld, S. N. Pandis, In Atmospheric Chemistry and Physics: From Air Pollution to Climate Change, John Wiley & Sons, New York (2012).

[2] I. Barnes, In Global Atmospheric Change and its Impact on Regional Air Quality, Springer Science & Business Media,Berlin (2012).

[3] J. G. Calvert et al., In Formaldehyde and Other Aldehydes, National Research Council, National Academy Press, Atlanta (1981).

[4] P. Carlier, H. Hannachi, G. Mouvier, Atmos. Environ. 20 (1986) 2079.

[5] T.P.M. Goumans, Mon. Not. R. Astrom. Soc. 413 (2011) 2615.

[6] K. Hiraoka, T. Sato, S. Sato, N. Sogoshi, T. Yokoyama, H. Takashima, S. Kitagawa, ApJ l. 577 (2002) 265-270.

[7] C. Oehlers, H.Gg. Wagner, H. Ziemer. J. Phys. Chem. A. 104 (2000) 10500.

[8] G. Friedrichs, D.F. Davidson, R.K. Hanson, Int J. Chem. Kinet.34 (2002) 374.

[9] B.A. Ridley, J.A. Davenport, L.J. Stief, K.H. Welge, J. Chem. Phys.57 (1972) 520.

[10] A.A. Westenberg, N. de Haas, J. Phys. Chem. 76 (1976) 2213.

[11] J. M. Bowman, Adv. Chem. Phys. 61 (1985) 115.

[12] J. M. Bowman, J. Phys. Chem. 95 (1991) 4960.

[13] R.B. Walker, E.F. Hayes, Reactive Scattering in the Bending Corrected Rotating Linear Model. *In The Theory of Chemical Reaction Dynamics*; D. C. Clary, Ed.; D. Reidel Publishing Compagny: Dordrecht, 1985, 105.

[14] B. Kerkeni, D.C. Clary, J. Chem. Phys. 120 (2004) 2308.

[15] B. Kerkeni, D.C. Clary, Chem. Phys. Lett. 438 (2007) 1.

[16] S. T. Banks, D. C. Clary, J. Chem. Phys. 130 (2009) 024106.

[17] H.F. von Horsten, S.T. Banks, D.C. Clary, J. Chem. Phys. 135 (2011) 094311.

[18] S. M. Remmert, S. T. Banks, J. N. Harvey, A. J. Orr-Ewing, D. C. Clary, J. Chem. Phys. 134 (2011) 204311.

[19] X. Shan, D.C. Clary, Phys. Chem. Chem. Phys. 15 (2013) 1222.

[20] X. Shan, D.C. Clary, J. Phys. Chem. A, 118 (2014) 10134.

[21] I. Oueslati, B. Kerkeni, W. -Ü L. Tchang-Brillet, N. Feautrier, Chem. Phys. Lett. 624 (2015) 29.

[22] D.G. Truhlar, A.D. Isaacson, and B. C. Garrett, Generalized Transition State Theory. *The Theory of Chemical Reaction Dynamics*, Ed.; M. Baer CRC Press: Boca Raton, 1985, 65.

[23] R. T. Skodje, D.G. Truhlar, B.C. Garrett, J. Phys. Chem. 85 (1981) 3019.

[24] D.H. Lu et al., Comput. Phys. Commun. 71 (1992) 235.

[25] Y.P. Liu, G.C. Lynch, T.N. Truong, D.H. Lu, D. H. D.G. Truhlar, B.C. Garrett, J. Am. Chem. Soc. 115 (1993) 2408.

[26] M. Head-Gordon and T. Head-Gordon, Chem. Phys. Lett. 220 (1994) 122.

[27] D.E. Woon and T.H. Dunning, J. Chem. Phys. 98 (1993) 1358.

[28] M.J. Frisch, G.W. Trucks, H.B. Schlegel *et al.*, Gaussian 09, Revision A.02, Gaussian, Inc., Wallingford CT, 2009.

[29] M.D. Halls, H.B. Schlegel, J. Chem. Phys. 109 (1998) 10587.

[30] G. Friedrichs, D.F. Davidson, R.K. Hanson, Int. J. Chem. Kinet. 36 (2004) 157.

[31] K. Yamada, T. Nakagawa, K. Kuchitsu, Y. Morino, J. Mole. Spectros. 38 (1971) 70.

[32] G. Herzberg, Electronic spectra and electronic structure of polyatomic molecules,Van Nostrand, New York (1966) 134.

[33] K.P. Huber, G. Herzberg, Molecular Spectra and Molecular Structure. IV. Constants of Diatomic Molecules, Van Nostrand Reinhold Co., New York (1979) 716.

[34] S. Dasgupta, T.Yamasaki, W.A. Goddard, J. Chem. Phys. 104 (1996) 2898.

[35] A.V. Marenich, J.E. Boggs, J. Phys. Chem. A, 107 (2003) 2343.

[36] E. Henon, F. Bohr, Chem. Phys. Lett. 342 (2001) 659.

[37] T. Shimanouchi, Tables of Molecular Vibrational Frequencies, Consolidated Volume I, National Bureau of Standards, (1972).

[38] K.K. Murray, T.M. Miller, D.G. Leopold, W.C. Lineberger, J. Chem. Phys. 84 (1986) 2520.

[39] I.N. Levine. In Molecular Spectroscopy, Wiley, NewYork (1975).

[40] J.A. Pople, M. Head-Gordon, K. Raghavachari, J. Chem. Phys., 87 (1987) 5968.

[41] T.B. Adler, G.Knizia, H.J. Werner, J. Chem. Phys., 127 (2007) 221106.

[42] B. Ruscic, J. Phys. Chem. A, 119 (2015) 7810.

[43] K. Fukui, Acc. Chem. Res. 14 (1981) 363.

[44] E. Rosenman, M.L. McKee. J. Am. Chem. Soc. 119 (1997) 9033.

[45] C.F. Jackels, Z. Gu and D.G. Truhlar, J. Chem. Phys. 102 (1995) 3188.

[46] J. Zheng, S. Zhang, B.J. Lynch, J.C. Corchado, Y.Y. Chuang, P.L. Fast, W.P. Hu, Y.P. Liu, G.C. Lynch, K.A. Nguyen et al. Polyrate, version 2010-A; University of Minnesota: Minneapolis, MN, 2010.

[47] D.H. Lu and D.G. Truhlar, J. Chem. Phys. 99 (1993) 2723.

[48] B. Kerkeni, D.C. Clary, Chem. Phys. Lett. 421 (2006) 499.

[49] P.E. Gill, W. Murray, J. Numer. Anal. 15 (1978) 977.

[50] J.C. Light, R.B. Walker, J. Chem. Phys. 65 (1976) 4272.

[51] E.B. Stechel, R.B. Walker, J.C. Light, J. Chem. Phys. 69 (1978) 3518.

[52] J. M. Bowman, Theo. Chem. Acc. 108 (2002) 125.

[53] I. Oueslati, B. Kerkeni, A. Spielfiedel, W.-Ü L. Tchang-Brillet, N. Feautrier, J. Phys. Chem. A 118 (2014) 791.

[54] D.G. Truhlar and B.C. Garrett, Ann. Rev. Phys. Chem. 35 (1984) 159.

[55] Y.-Y. Chuang, D. Truhlar, J. Phys. Chem. A, 102 (1998) 242.